ON-LINE APPENDIX: CASE SERIES

Case 1

A male term neonate had prenatal detection of an interhemispheric venous varix with signs of thrombosis (On-line Fig 1). A large right-frontal DVA draining into this secondary partially thrombosed venous varix was diagnosed on postnatal MR imaging performed at 38.6 -week corrected age (On-line Fig 2*A–E*). DSA confirmed the characteristic appearance of a caput medusae in the corresponding region without associated arteriovenous shunting, draining into the inferior sagittal sinus through the venous varix (On-line Fig 2*F, -G*). Long-term anticoagulation was initiated. White matter signal abnormalities in the draining territory of the DVA were more evident around 2 months of age (On-line Fig 3*A–C*) and gradually decreased on follow-up MR imaging. At last brain MR imaging performed at 7.2 years of age, the patient showed complete resolution of parenchymal signal changes (On-line Fig 3*D–F*) with normal aterial spin-labeling signal in that region (On-line Fig 3*H*). Total recanalization of the interhemispheric venous varix was also depicted, with a corresponding reduction in caliber (On-line Fig 3*D, -G, -I*). A neurologic examination performed at last clinical follow-up had normal findings.

Case 2

A male term neonate had respiratory distress after birth. Postnatal ultrasound identified a linear hyperechogenic focus in the left parietal region suggestive of a DVA (On-line Fig 4*A, -B*). Brain MR imaging performed at 38.7-week corrected age confirmed the diagnosed and depicted foci of restricted diffusion and small hemorrhages in the surrounding parenchyma. A focal area of polymicrogyria was also noted in the DVA cortical drainage territory (On-line Fig 4*C–H*). Follow-up brain MR imaging after 2 months demonstrated resolution of the areas of restricted diffusion. Neurologic examination findings at 2.5 years were normal, and no seizures were reported.

Case 3

A female term neonate had prenatal detection of hemorrhage involving the vermis and right cerebellar region (On-line Fig 5*A–D*), which was confirmed on postnatal MR imaging performed at 39.9-week corrected age (On-line Fig 5*E–J*). Neuroimaging follow-up during the first months of life revealed progressive resorption of the hemorrhagic component, with identification of a subjacent diffuse left cerebellar developmental venous anomaly and adjacent dystrophic calcifications (On-line Fig 5*K*). Multiple CCMs were also detected in the cerebellum and brain stem. DSA confirmed the presence of contrast medium staining in the venous phase in the vermis and left cerebellar hemisphere, in keeping with a diffuse cerebellar DVA draining into both the superficial and deep venous system (On-line Fig 5*L*). At 3 months of age, brain MR imaging showed the presence of a new vascular masslike lesion at the level of the superior vermis, characterized by small hemorrhages and inhomogeneous contrast enhancement (On-line Fig 6), which slowly spontaneously regressed during the following months. Last follow-up MR imaging performed at 3 years of age showed further signs of interval improvement regarding both cerebellar hemorrhages and vermian vascular lesions, with only mild gliotic cerebellar changes, stable dystrophic calcifications, and CCMs (On-line Fig 7). Clinical follow-up at the same age revealed mild neurologic impairment (broad-based gait).

Case 4

A female term infant had a prenatal detection of ventriculomegaly. Postnatal ultrasound revealed progressive triventricular hydrocephalus. Brain MR imaging performed at 42-week corrected age identified a mesencephalic DVA with deep drainage as the obstructive cause of the Sylvian aqueduct (On-line Fig 8*A–F*), without other associated abnormalities. Endoscopic third ventriculostomy was performed, and longitudinal follow-up at 3.7 years of age revealed normalization of the ventricular size (On-line Fig 8*G–I*) and normal neurologic examination findings.

Case 5

A female term neonate had prenatal detection of a dural sinus malformation without associated signs of thrombosis (On-line Fig 9*A–D*). At birth, a right facial and orbital venous malformation was noted. Postnatal MR imaging performed at 42-week corrected age and follow-up MR imaging studies confirmed the presence of a dural sinus malformation, which spontaneously regressed for months, and revealed additional venous lesions with a segmental distribution, including a DVA (distributed in the cerebral hemispheres bilaterally and in the right cerebellar hemisphere) with venous congestion in the right temporal lobe and CCM (On-line Fig 9*E–H*). On the basis of the type and segmental distribution of the vascular lesions, the diagnosis of CVMS type 2 was assumed. At 2.5 years of age, the orbital venous malformation was complicated by massive hemorrhage, and there was a suspicion of an associated high-low arteriovenous malformation on MRA (On-line Fig 10). DSA confirmed the presence of a right superior orbital fissure AVF (On-line Fig 10), which was treated with multiple embolization procedures along with the facial venous malformation, which was treated with several sessions of sclerotherapy. Longitudinal neuroimaging assessment at 8.2 years of age showed a mixed evolution of brain DVA complications, including interval reduction of WM abnormalities with residual small focal gliosis in the right temporal lobe and interval growth of the supratentorial CCM (On-line Fig 11). Neurologic examination findings at that age were normal.

Case 6

A female term neonate had mild signs of hypoxic-ischemic encephalopathy. Brain MR imaging and head CT performed at 39-week corrected age revealed a cerebral bihemispheric DVA with diffuse T2* hypointensity and hyperdensity of the right frontoparietal and left parietal WM (On-line Fig 12*A–D*). Follow-up brain MR imaging and head CT performed at 11 months demonstrated almost complete regression of the

T2* signal alterations with bilateral scattered areas of WM gliosis in the cerebral hemispheres, without associated calcifications (On-line Fig 12*E–H*). Neurologic examination revealed moderate developmental delay.

Case 7

A female was born preterm at 28 weeks' gestational age due to premature rupture of the membranes (<12 hours) from a vaginal birth. Pregnancy was not expected, with a history of smoking, alcohol consumption, use of ibuprofen, ketoprofen, and anticonception pills. Brain MR imaging was performed at 33-week corrected age due to postnatal detection of a right parietal linear hyperechogenic focus in keeping with a DVA on cUS and confirmed the presence of a parietal DVA with associated venous ischemic WM lesions and polymicrogyria. Other focal areas of polymicrogyria were also noted as well as open-lips schizencephaly bordered by hemosiderin and partial septum pellucidum agenesis (On-line Fig 13).

On-line Table: Global and subgroup baseline clinical characteristics

	All Cases ($n = 41$)	c-DVA Neonates ($n = 15$) (36.6%)	u-DVA Neonates ($n = 26$) (63.7%)	*P* Value[c]
Gestational age (median) (IQR) (wk)	38 (30.8–39.1)	39 (38–39)	33.9 (30.1–39)	.05
Prematurity (%)	19 (46.3)	3 (20)	16 (61)	.02
Corrected age first MR imaging (mean) (SD) (wk)	39.9 (2.2)	39.6 (2.3)	40.1 (2.1)	.44
Cesarean delivery (%)	22 (53.7)	5 (33)	17 (65.4)	.06
Twin pregnancy (%)	6 (14.6)	0 (0)	6 (23.1)	.07
Apgar score 1 (%)[a]				.75
<7	16 (40)	5 (33.3)	11 (42.3)	
7–10	24 (60)	9 (66.6)	15 (57.7)	
Apgar score 5 (%)[a]				1
<7	3 (7.5)	1 (7.1)	2 (7.7)	
7–10	37 (92.5)	13 (92.9)	24 (92.3)	
Imaging indication (%)				.005
Prenatal imaging abnormalities	11 (26.8)	7 (46.7)	4 (15.4)	
Neonatal complications	10 (24.4)	6 (40)	4 (15.4)	
Preterm screening	18 (43.9)	2 (13.3)	16 (61.5)	
Congenital CMV infection	2 (4.9)	0 (0)	2 (7.7)	
Multiple DVAs (%)	8 (19.5)	7 (46.7)	1 (3.8)	.002[d]
Craniofacial vascular lesions (%)	5	4[b]	1[b]	.02

Note:—CMV indicates cytomegalovirus.

[a] Apgar score is missing in 1 neonate.

[b] Including 1 patient with a diagnosis of cerebrofacial venous metameric syndrome.

[c] *P* values for group comparisons were determined by χ^2 or Fisher exact tests for categoric variables and independent samples *t* tests for continuous variables, as appropriate.

[d] Value statistically significant (statistical significance was set at $P < .005$ after Bonferroni correction for multiple comparisons).

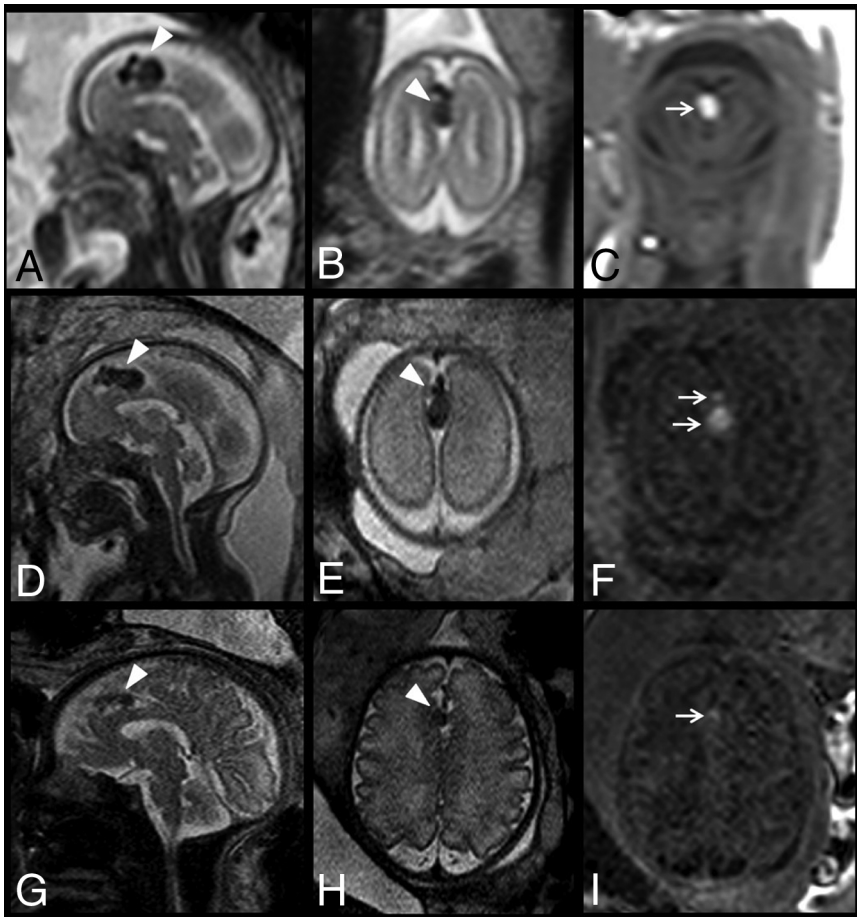

ON-LINE FIG 1. Fetal MR imaging of patient 1 performed at 20 (*A–C*), 24 (*D–F*), and 32 (*G–I*) weeks' gestational age. Single-shot FSE T2WI (*A, B, D, E, G, H*) and T1WI (*C, F, I*) demonstrate a dilated vascular structure in the anterior interhemispheric fissure, compatible with a venous varyx (*arrowheads*), with signs of thrombosis that progressively reduced in size with time (*arrows*).

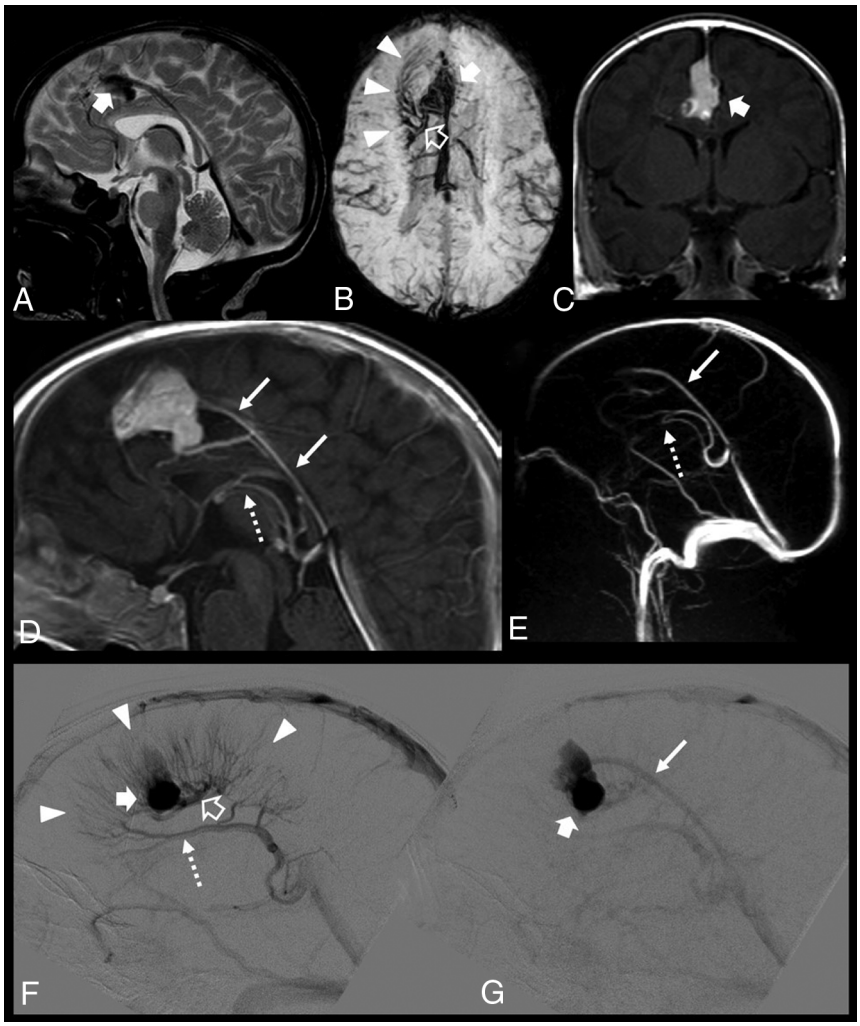

ON-LINE FIG 2. Postnatal brain MR imaging and DSA in patient 1. Sagittal T2WI (*A*), axial SWI (*B*), coronal (*C*) and sagittal contrast-enhanced T1WI (*D*), MRV (*E*), and DSA (*F* and *G*), sagittal angiograms in the venous phase. There are multiple dilated veins with a caput medusae morphology (*arrowheads*) in the right frontal lobe, radially converging into a large transmedullary collector vein (*empty arrows*), which, in turn, drains toward a partially thrombosed median varyx (*thick arrows*) and then to the inferior sagittal sinus (*arrows*). Note an additional venous collector draining into the right internal cerebral vein (*dotted arrows*).

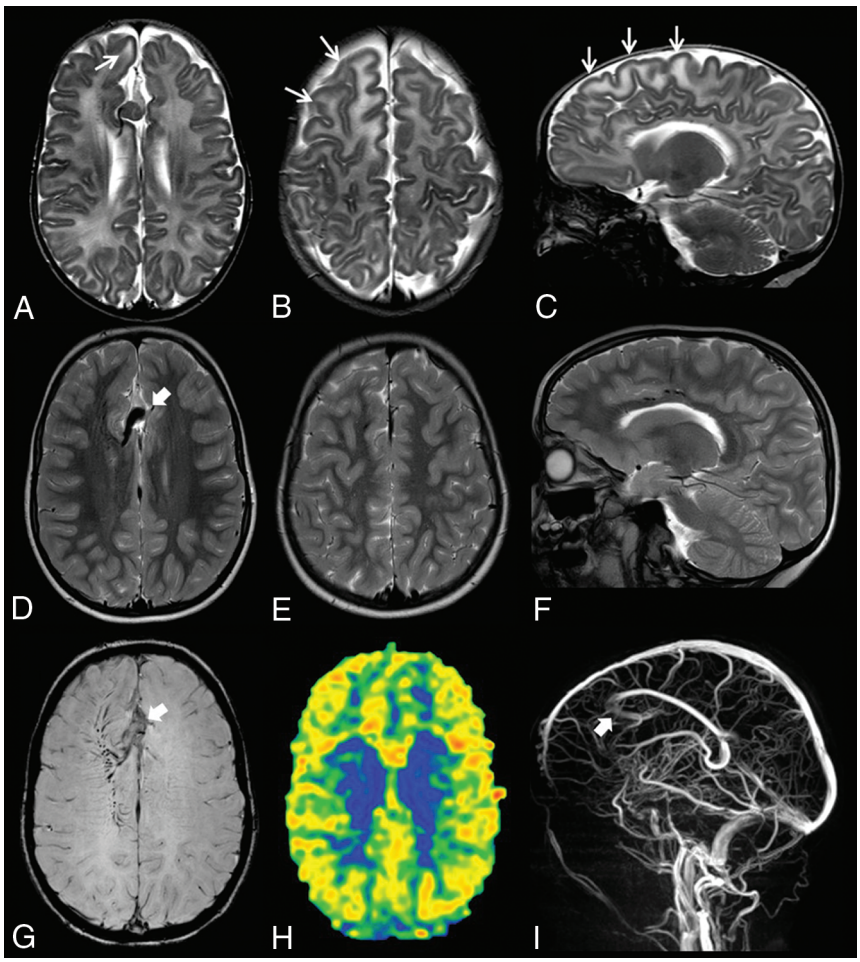

ON-LINE FIG 3. Follow-up brain MR imaging of patient 1 performed at 2 months (*A–C*) and 7 years of age (*D–I*). Axial (*A* and *B*) and sagittal (*C*) T2WI demonstrates increased signal in the WM surrounding the right frontal developmental venous anomaly compared with the remaining cerebral parenchyma (*arrows*). Corresponding axial T2WI (*D* and *E*), sagittal T2WI (*F*), and SWI (*G*) obtained at 7 years of age show complete resolution of WM signal abnormalities and progressive reduction in the size of the interhemispheric venous varyx (*thick arrows*). *H*, Axial 3D pseudocontinuous arterial spin-labeling map depicts symmetric perfusion of the frontal parenchyma. *I*, MRV, sagittal view, reveals venous flow signal in the draining varix, confirming almost complete resolution of the venous thrombosis (*thick arrow*).

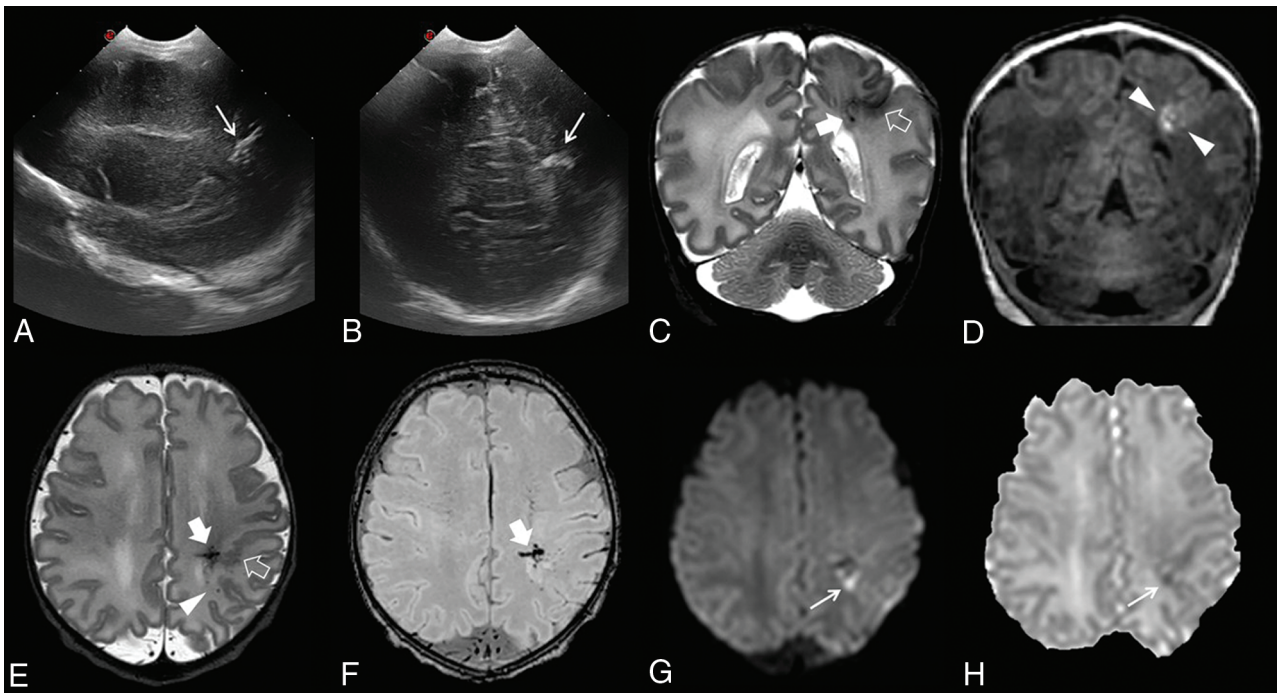

ON-LINE FIG 4. Neonatal cerebral ultrasound (*A* and *B*) and brain MR imaging (*C–H*) of patient 2. Sagittal (*A*) and coronal (*A*) cerebral sonograms identify a linear hyperechogenicity in the left parietal region (*thin arrows*), raising the suspicion of a developmental venous anomaly. Coronal T2WI (*C*) and T1WI (*D*) and axial T2WI (*E*) and SWI (*F*) confirm a developmental venous anomaly with deep drainage (*thick arrow*) and adjacent focal polymicrogyria (*empty arrow*). Note the presence of punctate hemorrhages, hyperintense on T1WI and hypointense on T2WI, in the same region (*arrowheads*). Axial DWI (*G*) and ADC map (*H*) show additional foci of restricted diffusion in the draining territory of the developmental venous anomaly (*thin arrows*).

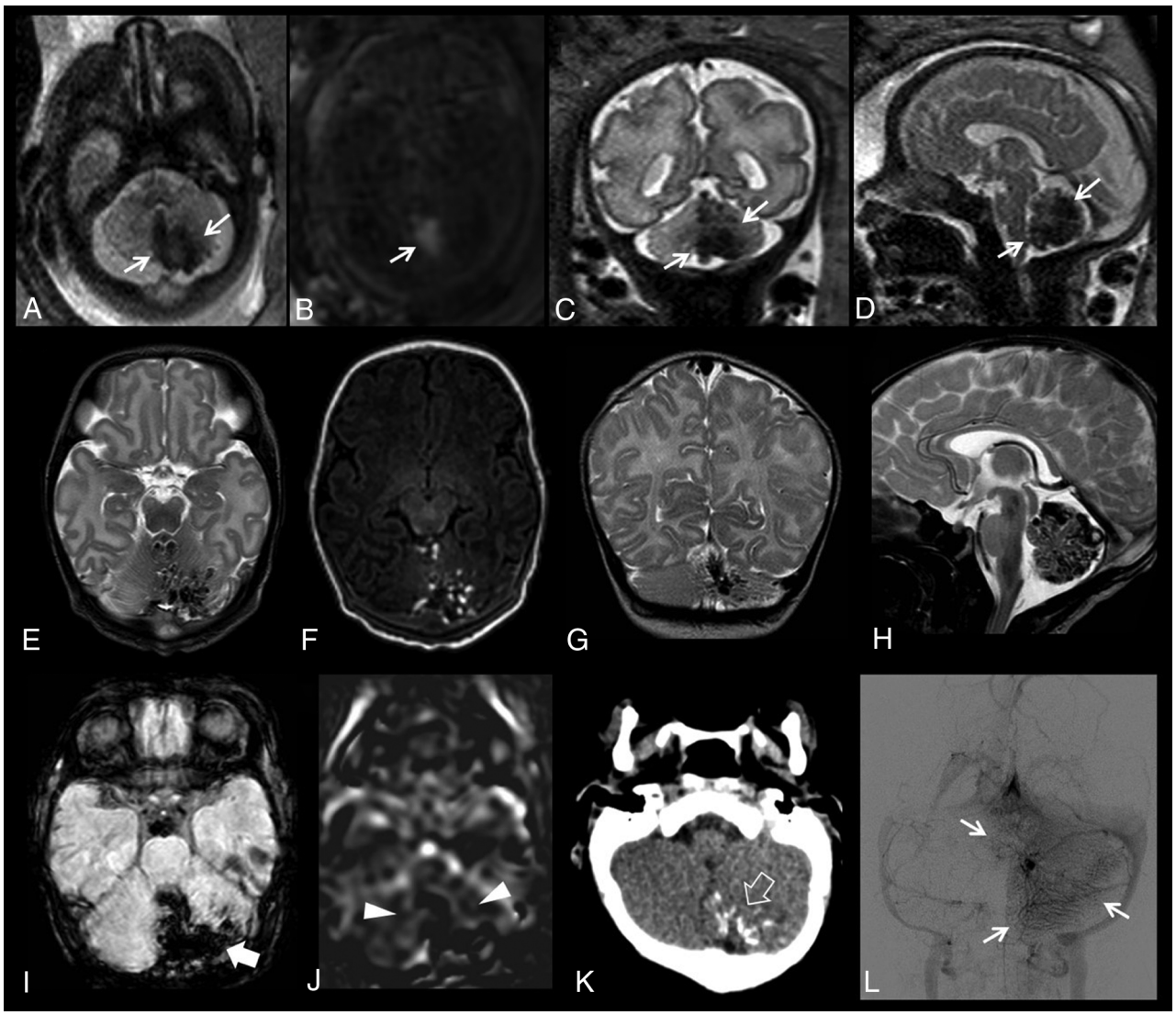

ON-LINE FIG 5. Fetal MR imaging of patient 3 performed at 31 weeks' gestation (*A–D*); axial single-shot FSE T2WI (*A*), axial T1WI (*B*), coronal (*C*) and sagittal (*D*) single-shot FSE T2WI. There are lobulated T2-hypointense and T1-hyperintense lesions in the vermis and left cerebellar hemisphere suggestive of parenchymal hemorrhage (*arrows*). Postnatal brain MR imaging performed at 6 days of age (*E–J*): axial T2WI (*E*) and T1WI (*F*), coronal (*G*) and sagittal (*H*) T2WI; axial SWI (*I*); and 3D pseudocontinuous arterial spin-labeling (*J*). There are extensive blooming artifacts on SWI (*thick arrow*), without an increased arterial spin-labeling signal (*arrowheads*). *K*, An unenhanced head CT scan demonstrates multiple calcifications in the inferomedial left cerebellar region (*empty arrow*). *L*, Coronal DSA in the late venous phase depicts persistent staining in the left cerebellar region, compatible with an underlying large, diffuse developmental venous anomaly (*arrows*).

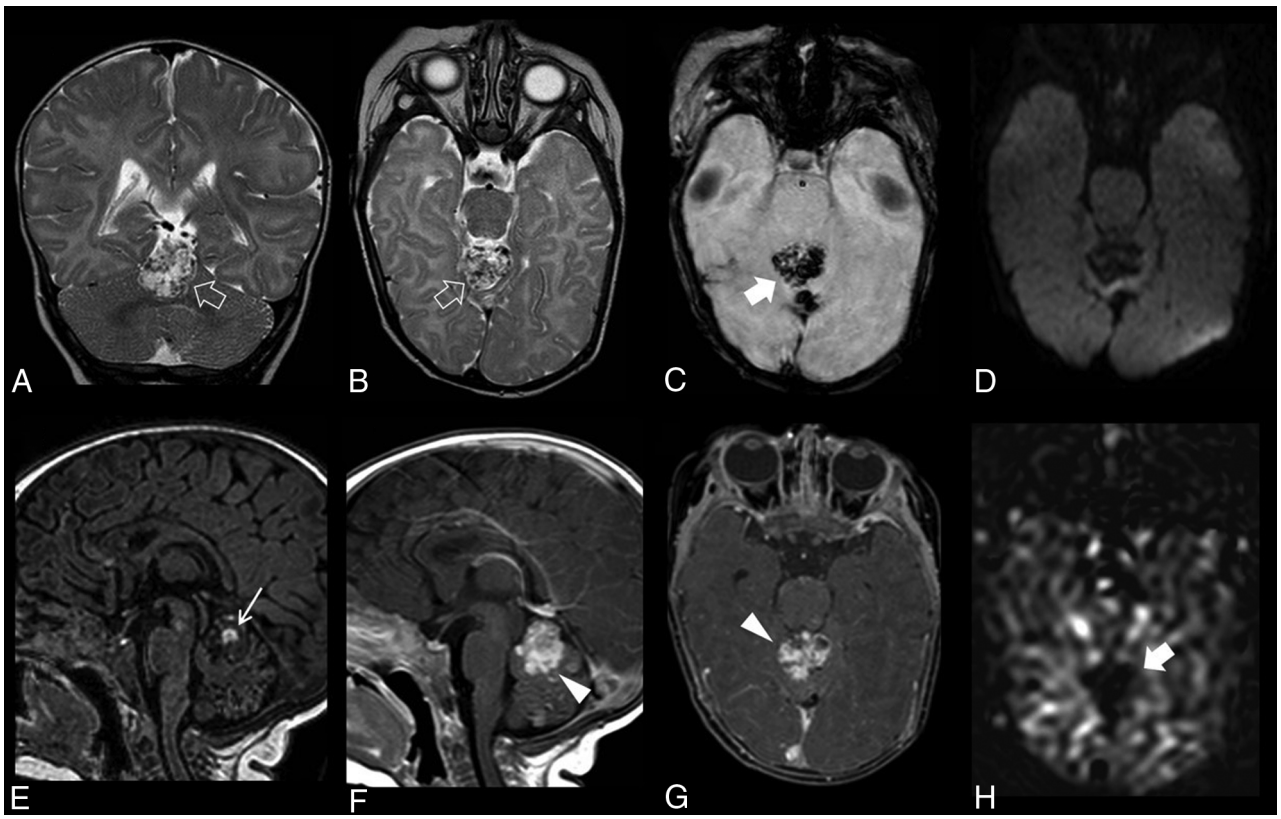

ON-LINE FIG 6. Follow-up brain MR imaging of patient 3 performed at 3 months of age. Coronal (*A*) and axial (*B*) T2WI identifies a new, heterogeneous expansive lesion in the superior vermis (*empty arrows*) with associated blooming artifacts on axial SWI (*C*, *thick arrow*). This mass does not present with hyperintensity of DWI *b*=1000 images (*D*), but a focal inner area of spontaneous hyperintensity is detected on sagittal T1-weighted images (*E*, *arrow*). Postgadolinium sagittal (*F*) and axial (*G*) T1WI shows intense enhancement of this likely vascular pseudomass (*arrowheads*). *H*, 3D pseudocontinuous aterial spin-labeling reveals reduced signal within the superior vermian lesion (*thick arrow*) and no areas of increased signal in the surrounding cerebellar parenchyma.

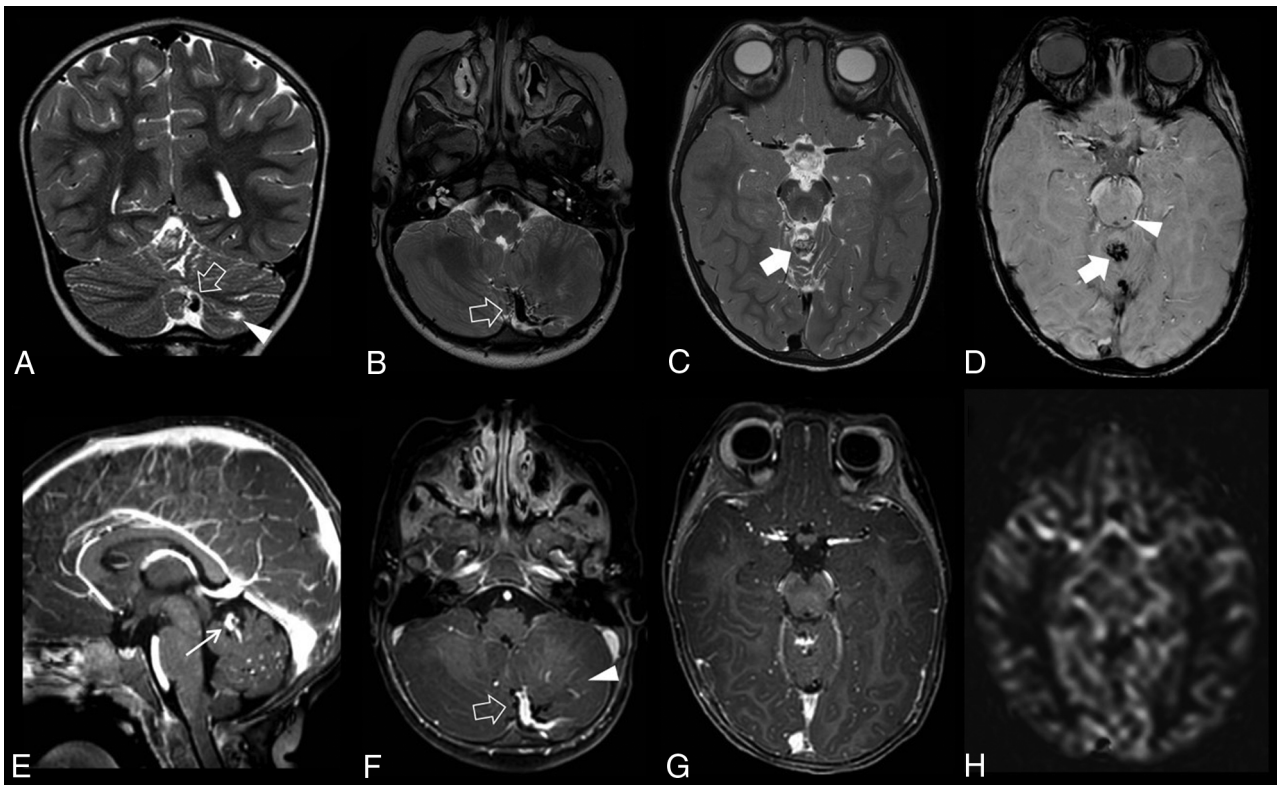

ON-LINE FIG 7. Last brain MR imaging of patient 3 performed at 3 years of age. Coronal (*A*) and axial (*B*) T2WI demonstrates complete regression of the multiple cerebellar hemorrhagic lesions with residual gliotic changes in the left cerebellar hemisphere (*arrowhead*). A large DVA venous collector is now visible (*empty arrows*). Axial T2WI (*C*) and SWI (*D*) at a higher level and contrast-enhanced sagittal TIWI (*E*) reveal spontaneous subtotal regression of the vascular pseudomass with a small residual nodular lesion characterized by hemosiderin deposits (*thick arrow*) and contrast enhancement (*arrow*). Note the small cavernoma in the left posterior midbrain (*arrowhead*). *F* and G, After gadolinium injection, the left cerebellar venous radicles (*arrowheads*) and major collector (*empty arrow)* of this developmental venous anomaly draining to the left transverse sinus are better depicted. *H*, 3D pseudocontinuous aterial spin-labeling confirms no increased signal at the level of the residual superior vermian masslike lesion.

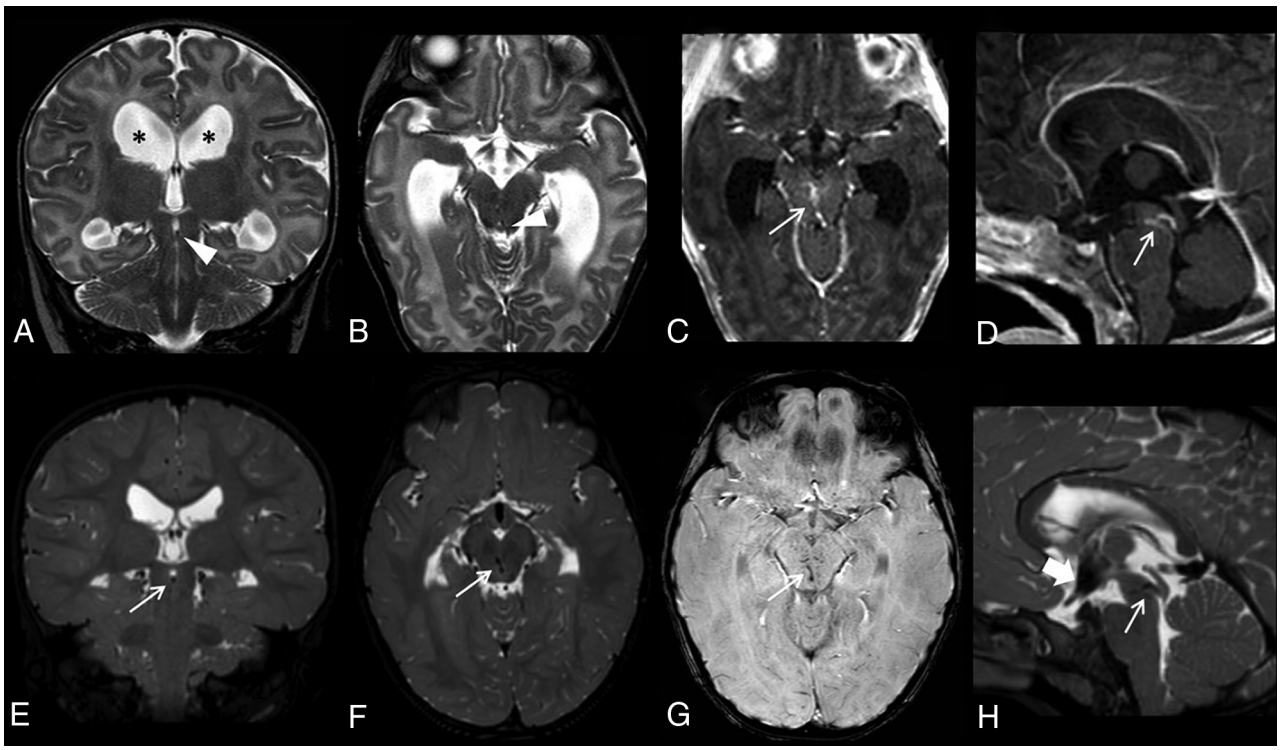

ON-LINE FIG 8. Neonatal brain MR imaging of patient 4 (*A–D*). Coronal (*A*) and axial (*B*) T2WI depicts diffuse enlargement of the supratentorial ventricular system (*asterisks*), in keeping with obstructive hydrocephalus. There is also absence of the normal CSF flow signal within the cerebral aqueduct, with a small vascular flow void in the inferior aqueduct (*arrowheads*). *C* and *D*, On postcontrast T1WI, small venous radicles and a slightly more dilated venous collector are depicted in the mesencephalon (*arrows*), in keeping with a DVA causing focal acqueductal obstruction. Postendoscopic third ventriculostomy brain MR imaging performed at 3.7 years of age (*E–H*). Coronal (*E*), axial (*F*), and sagittal (*H*) 3D T2WI reformats and axial SWI (*G*) confirm the presence of the mesencephalic developmental venous anomaly (*arrows*) and show interval resolution of the supratentorial hydrocephalus. A prominent CSF flow void is evident in the third ventricle floor, in keeping with patency of the third ventriculostomy (*thick arrow*).

ON-LINE FIG 9. Fetal MR imaging of patient 5 performed at 20 weeks' gestational age (*A–D*). Axial (*A* and *B*), coronal (*C*), and sagittal single-shot FSE T2WI identifies a markedly enlarged right transverse sinus in keeping with a dural sinus malformation (*thick arrows*), without features suggestive of intraluminal thrombosis. Note the mild right proptosis (*arrowheads*). Neonatal brain MR imaging of the same patient (*E–H*). Axial T2WI (*E*), contrast-enhanced T1WI (*F*), and SWI (*G*) show marked reduction of the dural sinus malformation (*thick arrows*) and additionally demonstrate venous malformations in the right intraorbital, periorbital, and masticatory spaces (*arrows*). Increased T2 hyperintensity in the right temporal white matter is also depicted (*asterisk*) associated with small, dilated veins corresponding to the caput medusae (*empty arrow*). *H*, DSA in the venous phase, coronal view, demonstrates patency of the enlarged right transverse sinus as well as persistent staining in the right parietal region, consisting of radially oriented veins converging into a single collector draining into the deep venous system, compatible with a developmental venous anomaly (*arrowhead*).

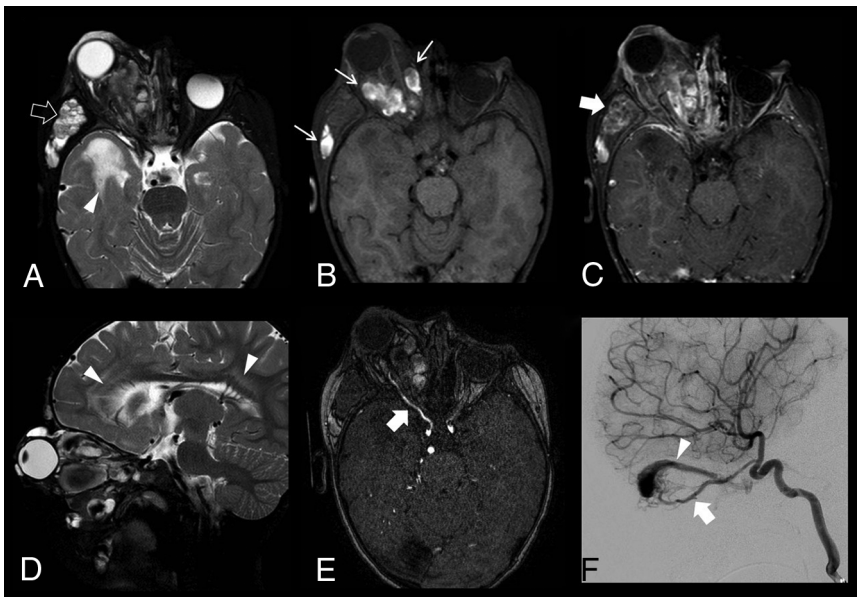

ON-LINE FIG 10. Follow-up brain MR imaging of patient 5 performed at 2.5 years of age. Axial T2WI (*A*) and fat-saturated pre- (*B*) and postcontrast (*C*) T1WI demonstrate marked enlargement of the facial/orbital venous-lymphatic malformations, leading to grade III right proptosis, mostly due to hemorrhagic evolution, with components characterized by multiple fluid-fluid levels (*empty arrow*), spontaneous T1 hyperintensity (*arrows*), and inhomogeneous contrast enhancement (*thick arrow*). Note the persistence of T2 hyperintensity in the right temporal WM and periventricular frontoparietal regions (*arrowheads*). *E*, Time-of-flight MRA reveals enlargement of the right ophthalmic artery, indicative of an intraorbital arteriovenous shunt. *F*, DSA in the arterial phase, sagittal view, confirms dilation of the right ophthalmic artery (*arrowhead*), with early filling of an intraorbital venous varyx and ophthalmic vein (*thick arrow*) into the ipsilateral cavernous sinus.

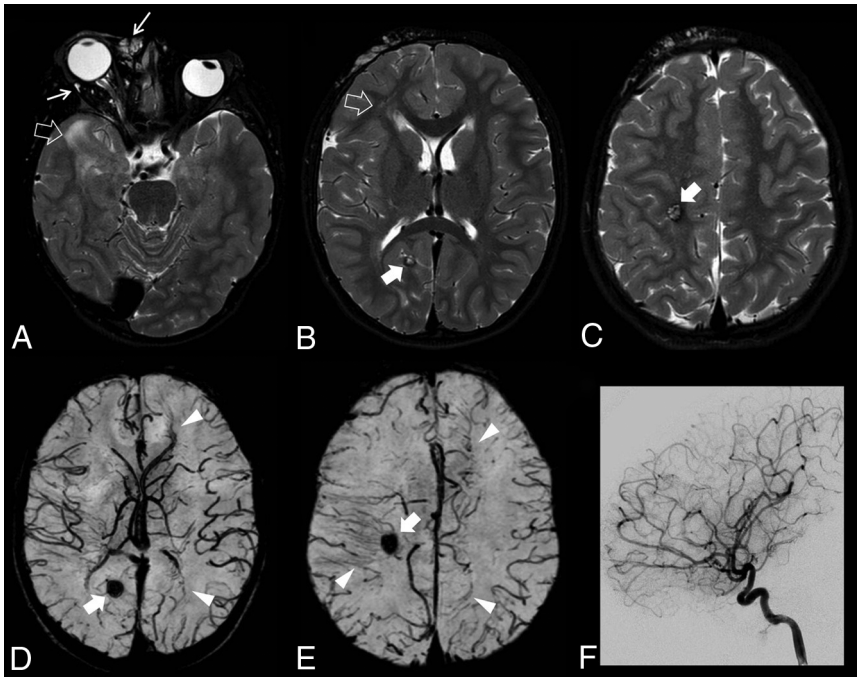

ON-LINE FIG 11. Last brain MR imaging of patient 5 performed at 8 years of age after multiple endovascular and percutaneous procedures: axial fat-saturated T2WI (*A–C*) and SWI (*D* and *E*). There is marked interval reduction in the size of the right facial/orbital venous malformations (*arrows*) and right proptosis. The WM signal abnormalities have also partially regressed (*empty arrows*). Cerebral cavernous malformations are depicted in the right occipital and parietal regions (*thick arrows*). Multiple areas of dilated veins with a caput medusae morphology are detected in the right frontoparietal region and left mesial frontal and parietal regions (*arrowheads*), corresponding to multiple bilateral hemispheric developmental venous anomalies. *F*, DSA in the arterial phase, sagittal view, reveals complete occlusion of the arteriovenous fistula.

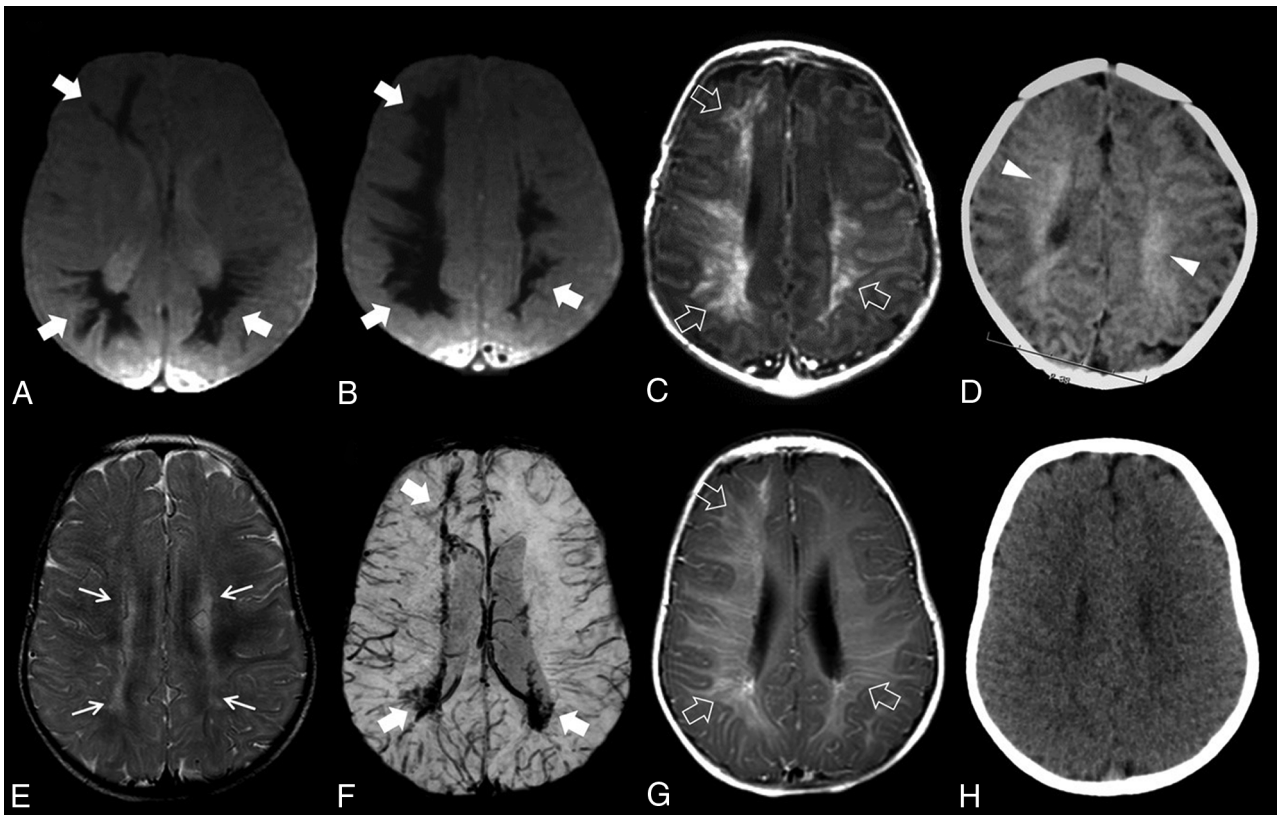

ON-LINE FIG 12. Brain MR imaging and CT scan of patient 6 at diagnosis (*A–D*) and at 11 months of age (*E–H*). Axial gradient-echo T2*WI (*A* and *B*) and contrast-enhanced T1WI (*C*) reveal multiple large developmental venous anomalies diffusively involving the right cerebral hemisphere and the left parietal region, with corresponding contrast enhancement (*empty arrows*) and extensive T2* hypointensity (*thick arrows*) in the cerebral white matter. *D*, Unenhanced head CT scan demonstrates bilateral cerebral white matter hyperdensity (*arrowheads*). *E–G*, Follow-up MR imaging at 11 months of age shows faint areas of increased periventricular and deep white matter T2-hyperintensity (*arrows*), compatible with residual gliosis. There is also marked reduction of blooming artifacts and contrast enhancement depicted on SWI (*F*, *thick arrows*) and post-gadolinium T1WI (*G*, *empty arrows*), respectively. *H*, An unenhanced head CT scan depicts normalization of cerebral WM density, without evident calcifications.

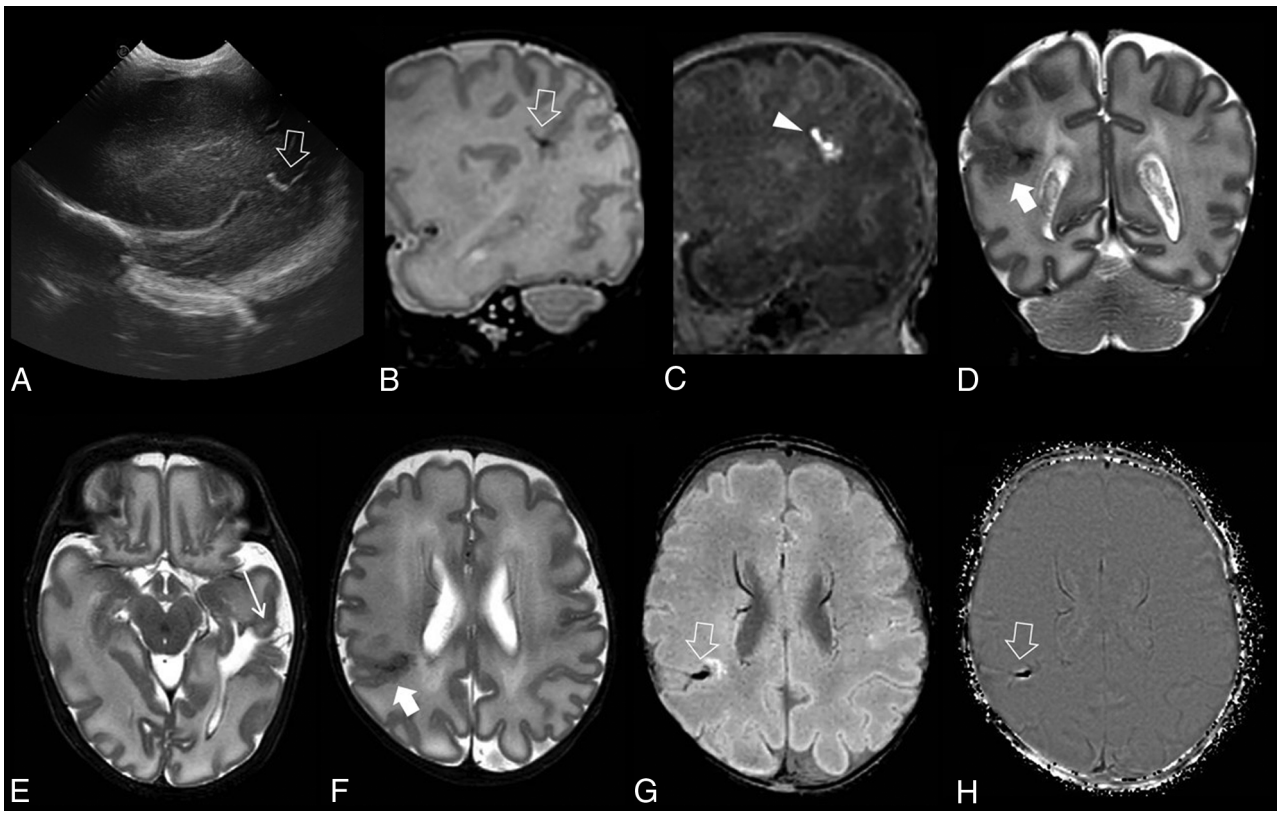

ON-LINE FIG 13. Cerebral ultrasound (*A*) and brain MR imaging (*B–H*) of patient 7. *A*, Sagittal cerebral ultrasonogram obtained shortly after birth identifies a linear hyperechogenicity in the right parietal region (*empty arrow*), raising the suspicion of a DVA. Sagittal T2WI (*A*) and T1WI (*B*) confirm the presence of a DVA with superficial venous drainage (*empty arrow*), as well as adjacent foci of microhemorrhage (*arrowhead*). Coronal (*D*) and axial (*E* and *F*) T2WI reveals a focal area of polymicrogyria at the same level (*thick arrow*), associated with an open-lip schizencephaly in the left temporal region (*arrow*). Axial SWI (*G*) and phase map (*H*) show the dilated DVA draining collector (*empty arrows*), without associated calcifications.